Extended abstract
AMS 89th Annual Meeting
11-15 January 2009, Phoenix, AZ

14.3 EVALUATION OF A NEW MULTIPLE-DOPPLER TORNADO DETECTION AND CHARACTERIZATION TECHNIQUE USING REAL RADAR OBSERVATIONS

Corey K. Potvin*[,1], Alan Shapiro[1], Tian-You Yu[2], and Jidong Gao[3]
[1]School of Meteorology, University of Oklahoma, Norman, OK
[2]School of Electrical and Computer Engineering, University of Oklahoma, Norman, OK
[3]Center for Analysis and Prediction of Storms, University of Oklahoma, Norman, OK

1. INTRODUCTION

Since the implementation of the WSR-88D network, several algorithms have been developed to aid forecasters in real-time identification of intense small and mesoscale vortices. The National Severe Storms Laboratory (NSSL) Mesocyclone Detection Algorithm (MDA; Stumpf et al. 1998) was designed to alert forecasters to the presence of supercell thunderstorms, which produce a large portion of tornadoes in the United States. The NSSL Tornado Detection Algorithm (TDA; Mitchell et al. 1998) calculates azimuthal shear of radial wind using adjacent radar resolution volumes, and identifies regions where shear exceeds a threshold. Unfortunately, the success of the TDA algorithm and others of its kind [e.g., Tornado Vortex Signature (TVS) algorithm, Crum and Alberty 1993] depends upon the chosen detection thresholds, the suitability of which is largely range- and storm-dependent. Thus, this approach may be subject to high false alarm rate or low probability of detection values.

The Velocity Track Display (VTD) technique and its variants (Lee et al. 1994; Roux and Marks 1996; Lee et al. 1999; Liou et al. 2006) were developed to retrieve the three-dimensional velocity field of a specific class of meteorologically significant flows: intense vortices. These techniques fit radial velocity data to a vortex model in order to recover key characteristics of the vortex flow. This capability distinguishes this approach from traditional dual-Doppler analysis, which does not constrain the retrieved wind field with a spatial vortex model and thus is not designed to retrieve vortex characteristics. Our method also adopts a vortex-fitting approach. More specifically, radial wind observations from two or more close-proximity Doppler radars with overlapping domains are fit to an analytical low-order model of a vortex and near-environment. The model control parameters include vortex location, size, intensity, and translation velocity. Our method is designed to capitalize upon the increased observational density and overlapping coverage of a CASA-like (Collaborative Adaptive Sensing of the Atmosphere; Mclaughlin et al. 2005; Brotzge et al. 2007) radar network to detect small-scale vortices and also to provide vortex characteristic estimates which may improve tornado nowcasting. The vortex parameters are obtained by minimizing a cost function which measures the discrepancy between the observed and model radial wind fields. By taking the translation of the system into account, the radar data can be used at their actual locations and times of acquisition.

Tests of the technique using analytically-generated and numerically-simulated tornadic wind fields can be found in Potvin et al. (2008). In this paper, the technique is applied to real dual-Doppler observations of tornadoes. The low-order model is introduced in section 2. The computation and minimization of the cost function is described in section 3. Section 4 describes tests using WSR-88D observations of an F4 tornado which struck central Oklahoma on 8 May 2003. Section 5 describes tests using high-resolution Doppler-on-Wheels observations of a relatively small tornado. A summary and plans for future work follow in section 6.

2. DESCRIPTION OF LOW-ORDER MODEL

The low-order model used in this study is comprised of four idealized flow fields: a uniform flow, linear shear flow, linear divergence flow, and modified combined Rankine vortex (MCRV; representing the tornado). The vortex and its environment are allowed to translate. Our use of the MCRV model is supported qualitatively by high-resolution mobile radar observations of tornadoes whose azimuthally-averaged tangential winds roughly followed this profile (Wurman and Gill 2000; Bluestein et al. 2003; Lee and Wurman 2005).

The Cartesian components of the linear flow fields (broadscale flow) are given by

$$V_x = a + b(y - v_b t) + c(x - u_b t),$$
$$V_y = d + e(x - u_b t) + f(y - v_b t), \qquad (1)$$

where *a*, *d* are constant flow components, *b*, *e* are shear parameters, *c*, *f* are divergence parameters, u_b, v_b are the translational velocity components of the broadscale fields, and *t* is time. It can be noted that (1) implicitly makes provision for a broadscale vortex since the Cartesian representation of a solid body vortex is $u = -\Omega y,\ v = \Omega x,$ where Ω is the (constant) vortex angular velocity. This broadscale vortex description is independent of the small-scale vortex model to be described next.

In a local cylindrical coordinate system centered on and translating with the modified combined Rankine vortex, the azimuthal velocity field v_θ and radial velocity field v_r are given by:

$$v_\theta = \begin{cases} \dfrac{r}{R} V_T, & r < R, \\ \dfrac{R^\alpha}{r^\alpha} V_T, & r \geq R, \end{cases} \qquad v_r = \begin{cases} \dfrac{r}{R} V_R, & r < R, \\ \dfrac{R^\beta}{r^\beta} V_R, & r \geq R, \end{cases} \qquad (2)$$

where

$$r = \sqrt{(x - x_0 - u_v t)^2 + (y - y_0 - v_v t)^2}\ , \qquad (3)$$

is the distance of a given (*x*, *y*) coordinate from the center of the vortex at time *t*. The vortex is described by seven parameters: initial vortex center location (x_0, y_0), radius of maximum wind *R*, maximum tangential velocity V_T, maximum radial velocity V_R, the radial decay rates α, β of the tangential and radial wind components, and the translational velocity components u_v , v_v. The model parameters are listed in Table 1.

To facilitate calculation of the radial (with respect to a radar) component of the model wind fields, the Cartesian components of the model wind fields are first obtained and then the radial component is extracted. Toward that end, the velocity **V** of the MCRV can be expressed in vortex-centered cylindrical coordinates (not radar coordinates) as the sum of its radial and tangential components, $\mathbf{V} = v_r \hat{r} + v_\theta \hat{\theta}$, where $\hat{r}$ and $\hat{\theta}$ are the unit vectors in the radial and azimuthal directions in the vortex cylindrical coordinate system, respectively. Figure 1 depicts the relationship between the Cartesian and vortex coordinate systems. The Cartesian components of **V** are computed as:

$$u = \hat{i} \cdot \mathbf{V} = v_r \cos\theta - v_\theta \sin\theta\ ,$$
$$v = \hat{j} \cdot \mathbf{V} = v_r \sin\theta + v_\theta \cos\theta\ . \qquad (4)$$

Formulae for *cosθ* and *sinθ* at arbitrary time *t* follow immediately from Fig. 1:

$$\cos\theta = \frac{x - x_0 - u_v t}{r}\ ,$$
$$\sin\theta = \frac{y - y_0 - v_v t}{r}\ .$$

Substituting these into (4) yields

$$u = \frac{x - x_0 - u_v t}{r} v_r - \frac{y - y_0 - v_v t}{r} v_\theta\ ,$$
$$v = \frac{y - y_0 - v_v t}{r} v_r + \frac{x - x_0 - u_v t}{r} v_\theta\ .$$

Substituting for v_r, v_θ from (2) and adding the linear flow fields (1) produces the Cartesian representation of the full model wind field:

$$u = \begin{cases} a + b(y - v_b t) + c(x - u_b t) + \dfrac{V_R}{R}(x - x_0 - u_v t) - \dfrac{V_T}{R}(y - y_0 - v_v t), & r < R, \\ a + b(y - v_b t) + c(x - u_b t) + \dfrac{R^\beta V_R (x - x_0 - u_v t)}{r^{\beta+1}} - \dfrac{R^\alpha V_T (y - y_0 - v_v t)}{r^{\alpha+1}}, & r \geq R, \end{cases}$$

$$v = \begin{cases} v = d + e(x - u_b t) + f(y - v_b t) + \dfrac{V_R}{R}(y - y_0 - v_v t) + \dfrac{V_T}{R}(x - x_0 - u_v t), & r < R, \\ \quad = d + e(x - u_b t) + f(y - v_b t) + \dfrac{R^\beta V_R (y - y_0 - v_v t)}{r^{\beta+1}} + \dfrac{R^\alpha V_T (x - x_0 - u_v t)}{r^{\alpha+1}}, & r \geq R. \end{cases}$$

Finally, solving for the radial component of the total velocity yields the model Doppler radar velocity, V_r^{mod}:

$$
\left.
\begin{aligned}
V_r^{mod} &= \cos\phi_n \sin\theta_n \left[a + b(y - v_b t) + c(x - u_b t) + \frac{V_R}{R}(x - x_0 - u_v t) - \frac{V_T}{R}(y - y_0 - v_v t) \right] + \\
&\quad \cos\phi_n \cos\theta_n \left[d + e(x - u_b t) + f(y - v_b t) + \frac{V_R}{R}(y - y_0 - v_v t) + \frac{V_T}{R}(x - x_0 - u_v t) \right] \\
&\quad r < R, \\
&= \cos\phi_n \sin\theta_n \left[a + b(y - v_b t) + c(x - u_b t) + \frac{R^\beta V_R (x - x_0 - u_v t)}{r^{\beta+1}} - \frac{R^\alpha V_T (y - y_0 - v_v t)}{r^{\alpha+1}} \right] + \\
&\quad \cos\phi_n \cos\theta_n \left[d + e(x - u_b t) + f(y - v_b t) + \frac{R^\beta V_R (y - y_0 - v_v t)}{r^{\beta+1}} + \frac{R^\alpha V_T (x - x_0 - u_v t)}{r^{\alpha+1}} \right] \\
&\quad r \geq R.
\end{aligned}
\right\} \qquad (5)
$$

where θ_n and ϕ_n are the azimuth and elevation angles, respectively, of the n^{th} radar (θ_n is measured clockwise from the north).

3. COST FUNCTION COMPUTATION AND MINIMIZATION

The (squared) discrepancies between the observed and model-predicted radial wind fields are summed over the spatial-temporal domains of N radars, each scanning in range r_n, azimuth θ and elevation angle ϕ. By taking the translation of the broadscale flow and vortex into account, discrepancy calculations for the radial wind model can be performed at the same locations and times as the observations.

Since radar resolution volumes increase in size with distance from the radar, Doppler velocity observations become representative of winds over a larger region as range increases. A range-weighting factor, r_n^2/r_{mean}^2, is introduced to account for this.

The cost function J accounting for the discrepancies between the observed and model-predicted radial wind fields is

$$
J \equiv \sum_{n=1}^{N} \sum_{m=1}^{M} \sum_{\phi} \sum_{\theta} \sum_{r_n} \left[\left(\frac{r_n}{r_{mean}} \right)^2 (V_r^{obs} - V_r^{mod})^2 \right], \qquad (6)
$$

where M is the total number of full volume scans (temporal sum) and r_n is the radial distance of a point from the n^{th} radar (the range-weighting factor is appropriately modified in experiments with real data as described above). J provides a useful way to quantitatively compare the quality of retrievals for different experiments, and, when appropriately normalized, can be used to calculate the mean model error per radar grid point.

The cost function J is minimized to retrieve the set of parameter values producing the least squares error in the model wind (best fit between model and observed winds). In view of (6) and the location of the model parameters in (5), our minimization problem is highly non-linear. Conjugate gradient minimization methods have proven useful for such problems. The minimization algorithm used in this technique is the Polak-Ribiere (1969) method, a robust and efficient variant of the Fletcher and Reeves (1964) algorithm. In both methods, the search direction is reset to that of steepest descent (with all previous direction and gradient information being discarded) every p iterations, where p is the number of model parameters.

As with other minimization techniques, multiple minima in J can prevent the global minimum from being reached. Local minima in the current problem can result from the intrinsic non-linearity of the problem, as well as from areas of missing data and departures of the observed wind field from the model.

An important example of the latter occurs when a tornado is collocated with a larger, non-tornadic vortex such as a mesocyclone. In such cases, the non-tornadic circulation, by virtue of its larger "footprint", may fit the low-order model better than the tornado itself, thus preventing the tornado from being detected. In order to address this problem, the minimization procedure was split into two steps. Figure 2 illustrates the procedure using one of the tests with numerically-simulated data described in Potvin et al. (2008). In step 1, the vortex model parameters are fixed at zero (except for R since this would introduce a "division by zero" computational issue), and the broadscale pa-

rameters are retrieved. In step 2, the radial components of the wind field retrieved in step 1 are subtracted from the observed radial wind fields, and the retrieval is repeated on the residual wind field. Since the flow retrieved in step 1 (and subtracted in step 2) is much more representative of the broadscale flow than of the tornadic flow, the tornadic component of the original flow dominates the residual field to be retrieved in step 2.

In order to further mitigate the problem of multiple minima, retrievals are performed for a multitude of first guess vortex centers. This increases the probability of detecting any tornadoes present within the analysis domain.

4. TESTS WITH WSR-88D OBSERVATIONS OF 8 MAY 2003 OKLAHOMA CITY TORNADO

4.1. Description of Dataset

On 8 May 2003, a supercell produced a long-lived F4 tornado in the southern portion of the Oklahoma City, Oklahoma metropolitan area. The tornado remained within the dual-Doppler domain of the KOKC (a Terminal Doppler Weather Radar) and KTLX radars (characteristics of both radars are listed in Table 2) throughout its lifetime, during which 0.5° elevation reflectivity and radial velocity scans were performed every ~5 min by KTLX and every ~1 min by KOKC. The tornado damage path and relative locations of KOKC and KTLX are depicted in Figure 3. A set of retrieval experiments was performed using data from five consecutive 0.5° KTLX scans along with one 0.5° KOKC scan taken within ~30-60 s of each KTLX scan. All velocity data used in the experiments were subjectively de-aliased. The proximity of the tornado to both radars (11-26 km) allowed observations to be collected at an azimuthal resolution characteristic of a CASA network. However, the range resolution of these data (150 m and 250 m) is coarser than that for a CASA radar (~50-100 m), and the large time interval between KTLX 0.5° scans required that retrievals be performed on single pairs of KTLX/KOKC scans rather than using multiple consecutive scans from each radar. Thus, the retrievals obtained in these experiments are presumably representative of, or somewhat poorer than, those which would have been obtained had the tornado been sampled by a network of CASA radars.

4.2. Selection of analysis domains

Using enough analysis domains to cover the entire dual-Doppler domain would, in the absence of a high performance computing cluster, require too much time for the technique to be applied operationally. Therefore, the technique was modified so that retrievals are performed only in regions identified as possibly containing tornado-like vortices. The process by which these regions are selected begins by identifying all pairs of azimuthally-adjacent radar gates which satisfy the following criteria: (1) azimuthal shear of radial velocity calculated between the two radar gates exceeds .05 s^{-1}; (2) the azimuthal distance between the two gates is less than 1 km; (3) radial velocity exceeds 25 m s^{-1} in at least one of the gates; and (4) < 20 % of the velocity data is missing within both 500 m and 1000 m of each of the gates. Criteria 1, 2 and 3 are intended to distinguish between tornado-like vortices and weaker or broader vortices. Criterion 4 was partly motivated by analytical experiments in which velocity data gaps produced spurious minima in J.

For each pair of radar gates satisfying all four criteria, the centroid of the two gates is stored. Since vortices always exhibit azimuthal shear signatures in the velocity fields of both radars, all centroids which are located within 2 km of another centroid in the other radar's domain are retained. All such points are then spatially grouped into clusters (since there may be multiple proximate points associated with the same vortex) whose centroids are calculated and stored. Each centroid corresponds to the center of a region over which the retrieval technique will be applied. A grid of nine first guesses (spacing = 500 m) for the vortex center (each serving as the center of an analysis domain over which the retrieval is applied) is subsequently calculated and input to the retrieval routine.

For each of the observational periods in this set of experiments, the only set of analysis domains to be objectively selected for input to the retrieval routine contained the tornado. Each set of nine retrievals required less than 1 min of computational time on a single AMD 2.6 GHz Opteron processor. It is currently unknown whether the analysis domain selection criteria are (or can be modified to be) sufficiently robust to simultaneously maintain a low number of retrieval sets and a high probability of detection over a wide range of tornado scenarios. If a large number of retrievals are needed, then parallel processing (one processor for each set of analysis domains) could be

used to produce acceptable computational wall clock times.

4.3. Detection criteria and vortex characterization

It was found in Potvin et al. (2008) that proximity of a vortex to a data boundary can result in spurious minima. This problem occasionally resulted in the retrieval of spurious vortices in preliminary experiments with real data (not shown). Therefore, in the experiments described below, retrievals were rejected if the magnitude of the retrieved vortex wind $\left(=\sqrt{v_r^2+v_\theta^2}\right)$ exceeded 20 m s^{-1} at the edge of the analysis domain.

A retrieved vortex is identified as a tornado if α < 1.0 and the radius of 30 m s^{-1} tangential winds, R_{30}, exceeds 200 m. The latter threshold is obtained by taking the mean of the smaller sampling interval for each radar (150 m and 250 m for KOKC and KTLX, respectively). The other criterion was motivated by the occasional retrieval of spurious vortices having unrealistically large (> 1.0) values of α. Such a rapid decline in v_θ with distance from the vortex center violates the Rayleigh (1916) instability condition and therefore may not be sustainable in actual tornadoes. This hypothesis is supported by high-resolution observational studies of tornadoes (e.g. Wurman and Gill 2000; Lee and Wurman 2005; Wurman and Alexander 2005) which have found that α typically varies between 0.6 and 0.8.

The mean retrieved vortex center and R_{30} are computed from the retrievals performed within each set of analysis domains. The latter parameter is intended to provide a useful estimate of the radius of damaging winds in the tornado. Mean retrieved values of R and V_T (as well as the remaining model parameters) are also calculated, but the tornado was not sufficiently resolved in these experiments for these estimates to be reliable. Since multiple tornado-like vortices may exist within a single set of analysis domains, the technique is designed such that retrieved vortices passing the detection criteria which are located > 1 km from the remaining detections have their characteristics calculated separately. In the experiments presented herein, the technique correctly identifies a single tornado.

4.4. Results

The technique successfully detected the tornado during all five observational periods (Table 3), which together spanned most of the tornado's lifetime. The mean distance between the vortex centers retrieved during each observational period (excluding the last period, during which only one detection was made) ranged from 57 m to 201 m, indicating that the technique was not unduly sensitive to errors in the first guess vortex center.

Though direct comparison of the mean retrieved vortex centers and R_{30} values to the observed damage path is hindered by several issues, most notably that the analysis domains in these experiments are ~ 100-220 m above the ground, the results are nevertheless encouraging. The mean retrieved vortex centers are all very nearly collocated with the observed tornado damage path (Figure 3). The mean retrieved R_{30} for each of the experiments are (in chronological order) 248 m, 296 m, 318 m, 265 m and 307 m, consistent with the observed maximum damage path width of ~ 650 m. The trend of R_{30} is similar to that of the damage path during the first four observational periods, while the fifth estimate is too large.

In order to assess how well the low-order model was able to reproduce the complexity of the input radial velocity fields, the mean retrieved wind field was compared to the observed wind field within the central analysis domain in each experiment. A representative comparison (experiment # 3) is shown in Figure 4. Naturally, the low-order model is unable to completely recover the intricate structure of the near-tornado radial wind field. However, the retrieved wind field does reasonably capture the primary structure of the tornado, at least on the scale of the observational data.

5. TESTS WITH DOPPLER-ON-WHEELS OBSERVATIONS OF 5 JUNE 2001 ATTICA, KS TORNADO

5.1. Description of Dataset

The technique was next applied to a dual-DOW (Doppler on Wheels; Wurman et al. 1997) dataset of a relatively small tornado which occurred near Attica, KS on 5 June 2001. Due to the presence of intervening precipitation, the tornado was never visually observed by the DOW team, and so the precise time period(s) during which the tornado occurred is unknown. The peak intensity of the tornado is also uncertain since no damage survey was performed. The vortex was estimated by a sheriff to be around 100 m in diameter,

though it is possible the tornado widened and/or narrowed during times in which it was not observed.

The azimuthal sampling interval for both radars averaged less than 0.4° and the radial sampling interval varied between 50 m and 75 m. Due to the very high observational density the radius of 25 ms^{-1} vortex tangential wind, R25, was used in the detection criteria rather than R30. Since the azimuthal spacing between observations was typically less than the radial spacing, the detection threshold for R25 was set to the mean azimuthal spacing between observations (rather than the mean radial spacing as in the previous set of experiments) within the analysis domain. The azimuthal distance between observations near the tornado averaged around 50 m.

The technique was applied to a single pair of radial velocity PPI scans for eight consecutive coordinated pairs of volume scans. Each pair of PPIs was selected such that the heights of the radar beams were within 100 m of each other in the vicinity of the tornado. The heights of the PPIs near the tornado were typically ~ 100-150 m AGL in these cases.

5.2. Modifications to Technique

In this set of tests, the low-order model was expanded to account for vertical shear of the broadscale flow. This is because the variation in height over the analysis domain in some of these experiments was potentially significant due to the proximity of the tornado to one of the radars.

During our experiments it was found that, even away from data boundaries, the technique occasionally retrieves an intense vortex where none is actually present in the data (not shown). Curiously, such spurious vortex retrievals tend to occur in regions of relatively weak flow. Therefore, in order to filter these false detections, vortices retrieved in regions in which (1) the maximum absolute Vr measured by both radars is less than 20 ms-1, or (2) the maximum absolute Vr measured by one radar is less than 15 ms-1, or (3) the maximum gate-to-gate radial wind difference is less than 10 ms-1 are automatically rejected by the algorithm. This is admittedly a rather ad-hoc solution to this problem. It is hoped that the cost function can be modified (perhaps, for example, by incorporating spectrum width data) to prevent these spurious vortex retrievals.

5.3. Results

Tornado detections were made at all of the eight times for which the algorithm was performed (Table 3). Again, it is not known at which times a tornado was actually occurring, however, inspection of the observed radial wind fields, some of which are shown in Figure 5, indicates that an intense vortex was indeed present at most or all of these times. The retrieved radial velocity fields generally compare favorably to the observations, although relatively poor broadscale flow retrievals may have prevented the most intense vortex in the analysis domain from being detected at time # 8. Both the retrieved radial velocity fields and plots of retrieved V_T and R_{25} over time (Figure 6) indicate that the algorithm captured trends in the size and resolvable intensity of the vortex reasonably well.

Due to the large values of radial velocity and shear present over a large area of the storm, the algorithm frequently performed retrievals in regions located well away from the suspected tornado. No detections were made in these cases except at time # 7. Inspection of the radial wind fields at this time reveals that an anticyclonic vortex may indeed be present at the location of the detection (Figure 7).

The observational resolution in these experiments is admittedly higher than in a typical CASA-like radar network. However, it should be borne in mind that the tornado being retrieved is relatively small (Alexander and Wurman 2008). Thus, the technique's ability to detect the tornado and characterize trends in its size and strength is encouraging.

6. SUMMARY AND FUTURE WORK

A new multiple-Doppler technique for identifying and characterizing tornadoes has been presented. The method consists of fitting radial wind observations to a low-order model of a tornado-like vortex and its near environment. The technique takes advantage of the enhanced density (and therefore spatial coverage and resolution) of a CASA-like radar network. The retrieval technique has previously been tested against analytically-generated observations as well as a high-resolution ARPS simulation of a tornado and surrounding wind field (not shown). In this work, the algorithm was applied to two sets of real dual-Doppler observations of a tornado. The technique exhibits skill not only in detecting tornado-like vortices within a CASA-like network, but also in retrieving the vortex location and wind field on

scales greater than or equal to that of the radar grid. Characteristics of retrieved vortices, if available to forecasters in real-time, could aid in the tornado warning process.

Spurious minima can pose a serious threat to the algorithm's ability to converge to the correct minimum, especially when the first guess model parameters (particularly the location of the vortex center) contain significant error. Boundary minima in $J(x_0, y_0)$ can occur near the edge of the analysis domain, and local minima can occur in other multi-dimensional cross-sections of J due to regions of missing data or deviations of the observed wind pattern from that described by the low-order model. An important special case of such a deviation is the presence of multiple vortices in the data. This local minima problem necessitates the use of multiple first guesses for the location of the vortex and of a two-step approach in which much of the larger-scale flow is retrieved and subtracted before a small-scale vortex retrieval is performed. The latter strategy is necessary in cases where a weaker and broader vortex-like circulation provides a better fit to the low-order model over an analysis domain than a collocated intense vortex. Finally, the stationarity of the low-order model parameters requires that the temporal analysis domain be limited in order to mitigate violation of the model in cases of rapid flow evolution.

Successful detection and characterization criteria (to be further developed in future work) need to account for non-uniqueness in the vortex parameters due to finite observational resolution and the mathematical nature of the low-order model. One preliminary approach tested herein is the inclusion in the detection criteria of retrieved vortex characteristics which are resolvable on larger scales than the vortex core. This approach demonstrated skill in distinguishing between tornadic and spurious retrieved tornado-like vortices in our experiments.

Due to computational constraints, it is not possible to apply the technique over the entire multiple-Doppler radar domain in real-time. Objective radial velocity criteria were therefore developed to identify sub-domains possibly containing tornadoes. These criteria will be further tested and refined through additional tests with real multiple-Doppler tornado observations.

Acknowledgements: We appreciate the contributions of the Doppler on Wheels crew including Curtis Alexander, MyShelle Bryant, Bob Conzemius, David Dowell, Steve McDonald, Kevin McGrath, Kevin Scharfenberg, Herb Stein, Josh Wurman and Pengfei Zhang during ROTATE (Radar Observations of Tornadoes and Thunderstorms Experiment) 2001. The work presented herein was primarily supported by NSF grant EEC-031347, through the Engineering Research Center (ERC) for Collaborative Adaptive Sensing of the Atmosphere (CASA).

REFERENCES

Alexander, C., and J. Wurman, 2008: Updated mobile radar climatology of supercell tornado structures and dynamics. Preprints, 24th Conf. on Severe Local Storms, Savannah, GA, Amer. Meteor. Soc.

Bluestein, H. B., W.-C. Lee, M. Bell, C. C. Weiss, and A. L. Pazmany, 2003: Mobile Doppler radar observations of a tornado in a supercell near Bassett, Nebraska, on 5 June 1999. Part II: Tornado-vortex structure. *Mon. Wea. Rev*., **131**, 2968–2984.

Brotzge, J., K. Brewster, V. Chandrasekar, B. Philips, S. Hill, K. Hondl, B. Johnson, E. Lyons, D. McLaughlin, and D. Westbrook, 2007: CASA IP1: Network operations and initial data. Preprints, 87th AMS Annual Meeting, San Antonio, TX, Amer. Meteor. Soc.

Crum, T. D., and R. L. Alberty, 1993: The WSR-88D and the WSR-88D Operational Support Facility. *Bull. Amer. Meteor. Soc*., **74**, 1669–1687.

Fletcher, R., and C.M. Reeves, 1964: Function minimization by conjugate-gradients. *Computer J*., **7**, 149-153.

Lee, W.C., and F.D. Marks, 2000: Tropical Cyclone Kinematic Structure Retrieved from Single-Doppler Radar Observations. Part II: The GBVTD-Simplex Center Finding Algorithm. *Mon. Wea. Rev*., **128**, 1925–1936.

——, W.-C., and J. Wurman, 2005: Diagnosed three-dimensional axisymmetric structure of the Mulhall tornado on 3 May 1999. *J. Atmos. Sci*., **62**, 2373-2393.

——, F. D. Marks, Jr., and R. E. Carbone, 1994: Velocity Track Display – A technique to extract real-time tropical cyclone circulations using a single airborne Doppler radar. *J. Atmos. Oceanic Technol*., **11**, 337–356.

——, J.-D. Jou, P.-L. Chang, and S.-M. Deng, 1999: Tropical cyclone kinematic structure retrieved from single Doppler radar observations. Part I: Interpretation of Doppler velocity

patterns and the GBVTD technique. *Mon. Wea. Rev.*, **127**, 2419-2439.

Liou, Y.-C., T.-C. Chen Wang, W.-C. Lee, and Y.-J. Chang, 2006: The retrieval of asymmetric tropical cyclone structures using Doppler radar simulations and observations with the Extended GBVTD technique. *Mon. Wea. Rev*., **134**, 1140-1160.

McLaughlin, D., V. Chandrasekar, K. Droegemeier, S. Frasier, J. Kurose, F. Junyent, B. Philips, S. Cruz-Pol, and J. Colom, 2005: Distributed Collaborative Adaptive Sensing (DCAS) for improved detection, understanding, and predicting of atmospheric hazards. Preprints, 85th AMS Annual Meeting, San Diego, CA, Amer. Meteor. Soc.

Mitchell, E. D., Vasiloff, S. V., Stumpf, J. G., Witt, A., Eilts, M. D., Johnson, J. T., and K. W. Thomas, 1998: The National Severe Storms Laboratory Tornado Detection Algorithm. *Wea. Forecasting*, **13**, 352–366.

Polak, E. And G. Ribiere, 1969: Note sur la convergence de methods de directions conjuguees. Rev. Franc. Informat. Rech. Operationnelle, **16**, 35-43.

Potvin C. K., Shapiro A., Yu T.-Y., Gao J., and Xue M., 2008: Using a low-order model to detect and characterize tornadoes in multiple-Doppler radar data. *Mon. Wea. Rev*., In Press.

Rayleigh, Lord (J. W. Strutt), 1916: On the dynamics of revolving flows. Proc. Roy. Soc. London, A93, 148-154.

Roux, F., and F. D. Marks, 1996: Extended velocity track display (EVTD): An improved processing method for Doppler radar observation of tropical cyclones. *J. Atmos. Oceanic Technol.*, **13**, 875–899.

Wurman, J., and S. Gill, 2000: Finescale radar observations of the Dimmitt, Texas (2 June 1995), tornado. *Mon. Wea. Rev*., **128**, 2135-2164.

——, and C. R. Alexander, 2005: The 30 May 1998 Spencer, South Dakota, Storm. Part II: Comparison of observed damage and radar-derived winds in the tornadoes. *Mon. Wea. Rev.*, **133**, 97–119.

——, Y. Richardson, C. Alexander, S. Weygandt, and P.-F. Zhang, 2007a: Dual-Doppler and single-Doppler analysis of a tornadic storm undergoing mergers and repeated tornadogenesis. *Mon. Wea. Rev*., **135**, 736–758.

——, J. Straka, E. Rasmussen, M. Randall, and A. Zahrai, 1997: Design and deployment of a portable, pencil-beam, pulsed, 3-cm Doppler radar. *J. Atmos. Oceanic Technol.*, **14**, 1502–1512.

Table 1. Low-order model parameters.

Parameter	Description
a ($m\ s^{-1}$)	Uniform flow
d ($m\ s^{-1}$)	
b (s^{-1})	Shear amplitudes
e (s^{-1})	
c (s^{-1})	Divergence amplitudes
f (s^{-1})	
u_b ($m\ s^{-1}$)	Broadscale field translation
v_b ($m\ s^{-1}$)	
R (m)	Radius of max wind
V_R ($m\ s^{-1}$)	Max radial, tangential wind
V_T ($m\ s^{-1}$)	
x_0 (m)	Vortex center
y_0 (m)	
u_v ($m\ s^{-1}$)	Vortex translation
v_v ($m\ s^{-1}$)	
α	Vortex wind decay
β	

Table 2. Selected characteristics of the KOKC and KTLX radars.

	Doppler Band	Beamwidth	Azimuthal Sampling	Range Sampling
KTLX	S	0.95°	1.0°	250 m
KOKC	C	1.0°	1.0°	150 m

Table 3. Number of tornado detections (out of nine retrievals) made in each of the May 8 2003 and 5 June 2001 experiments.

Experiment	Number of Detections
8 May 2003	
# 1	5
# 2	4
# 3	4
# 4	3
# 5	1
5 June 2001	
# 1	1
# 2	4
# 3	2
# 4	1
# 5	7
# 6	6
# 7	3
# 8	2

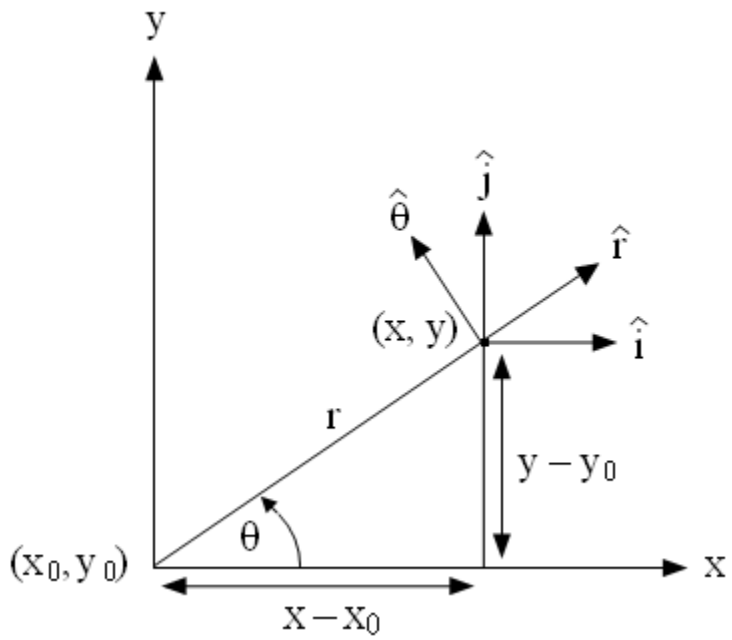

Fig. 1. Cartesian and cylindrical (vortex) coordinate systems defining model broadscale and vortex flows, respectively at t = 0. The vortex is initially located at x_0, y_0.

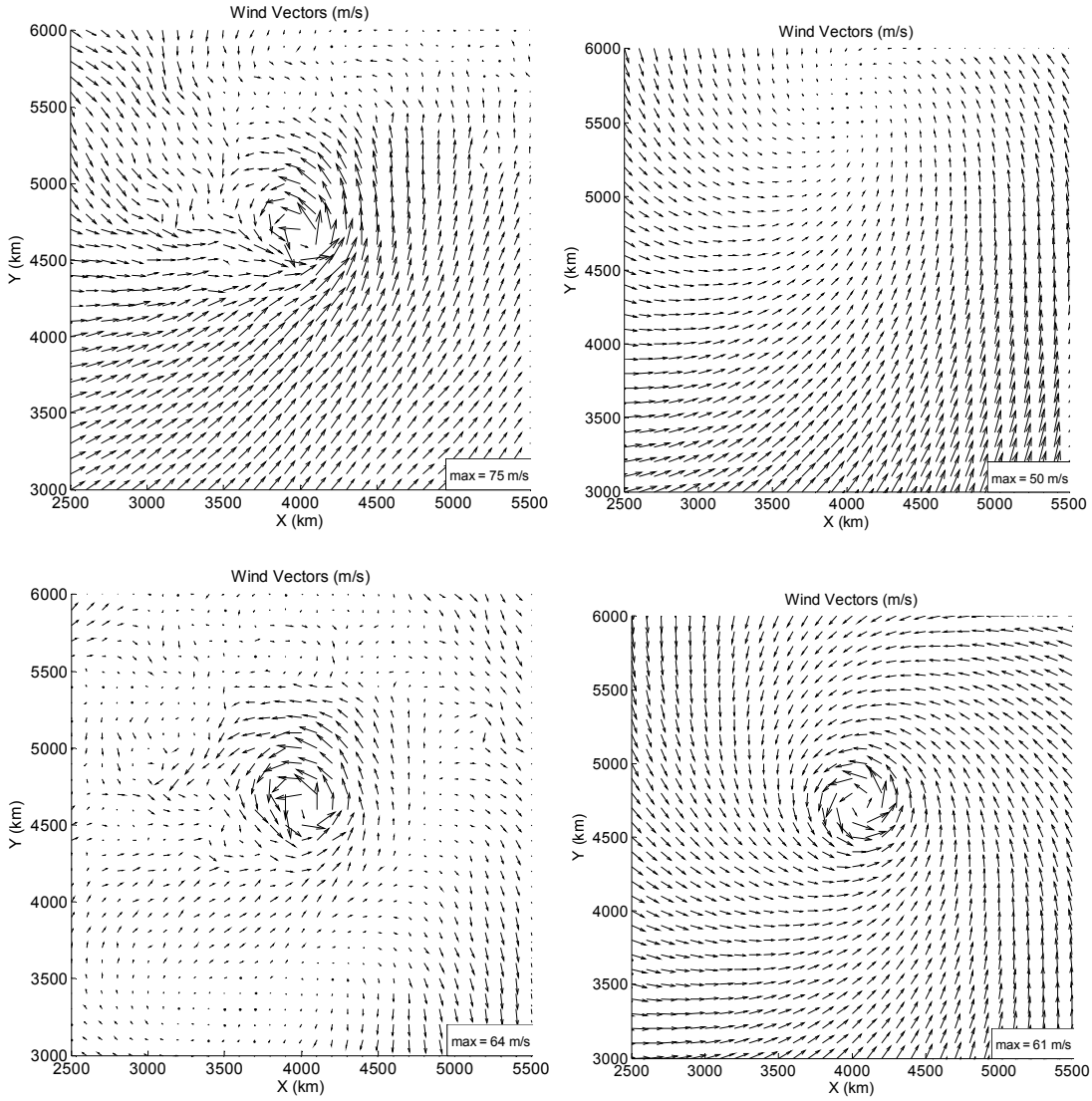

Fig. 2. Illustration of two-step retrieval procedure: (a) total wind field, (b) retrieved broadscale flow, (c) the vector difference (a)-(b), and (d) total retrieved flow.

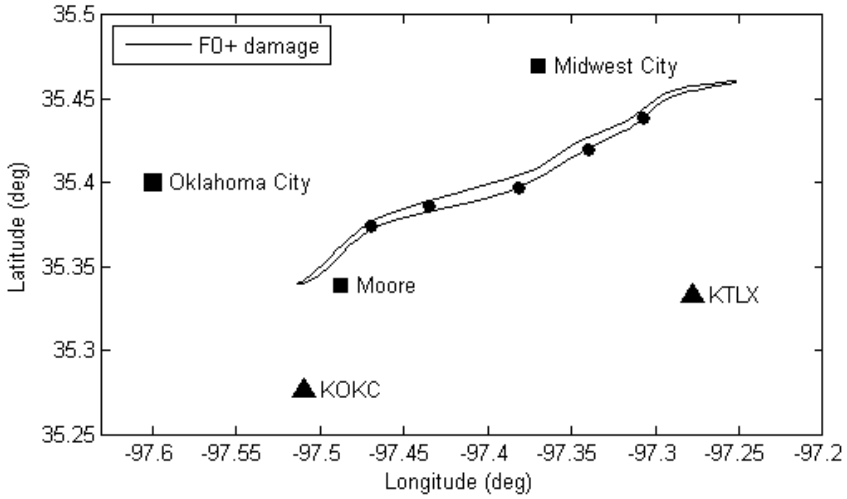

Fig. 3. Location of the tornado damage path (F0+) relative to KTLX and KOKC. The dots along the damage path indicate the tornado locations retrieved by the technique.

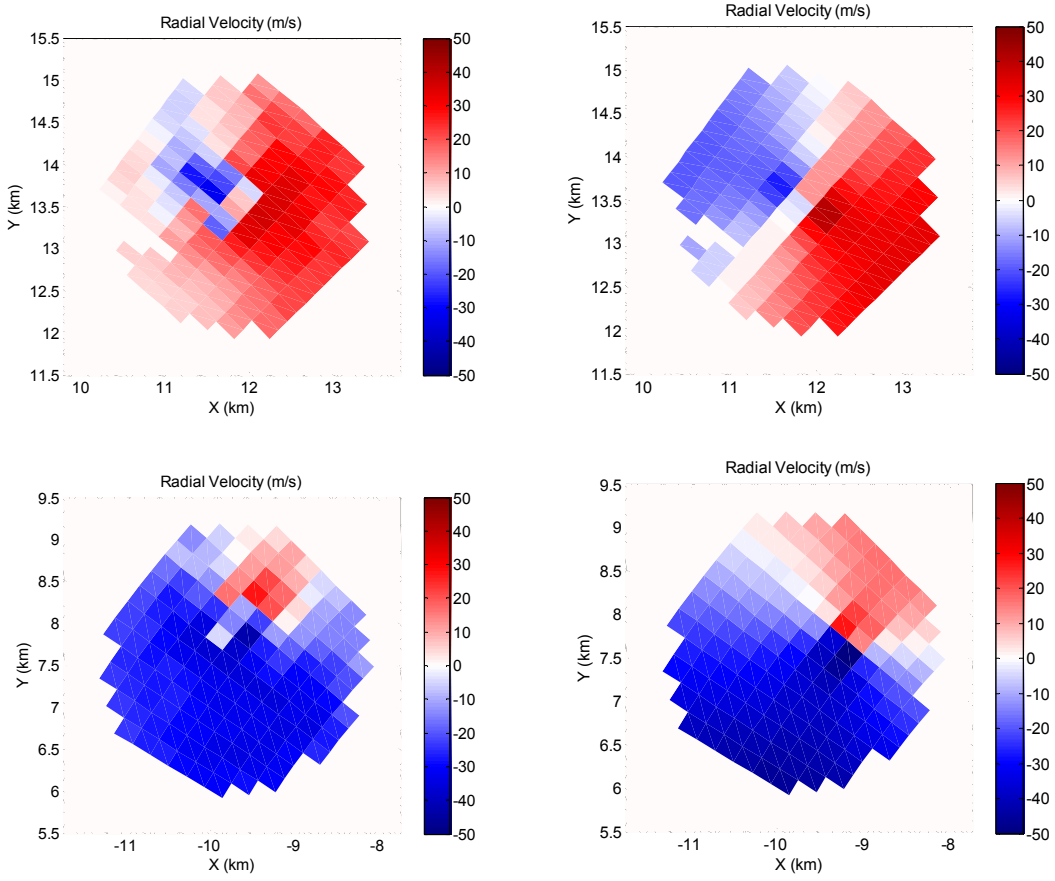

Fig. 4. KTLX (top left) and KOKC (bottom left) observed (left panels) vs. retrieved (right panels) radial velocities.

Fig. 5. Observed (left panels) and retrieved (right panels) radial velocity for DOW2 (top panels) and DOW3 (right panels) at four of the eight times at which retrievals were performed.

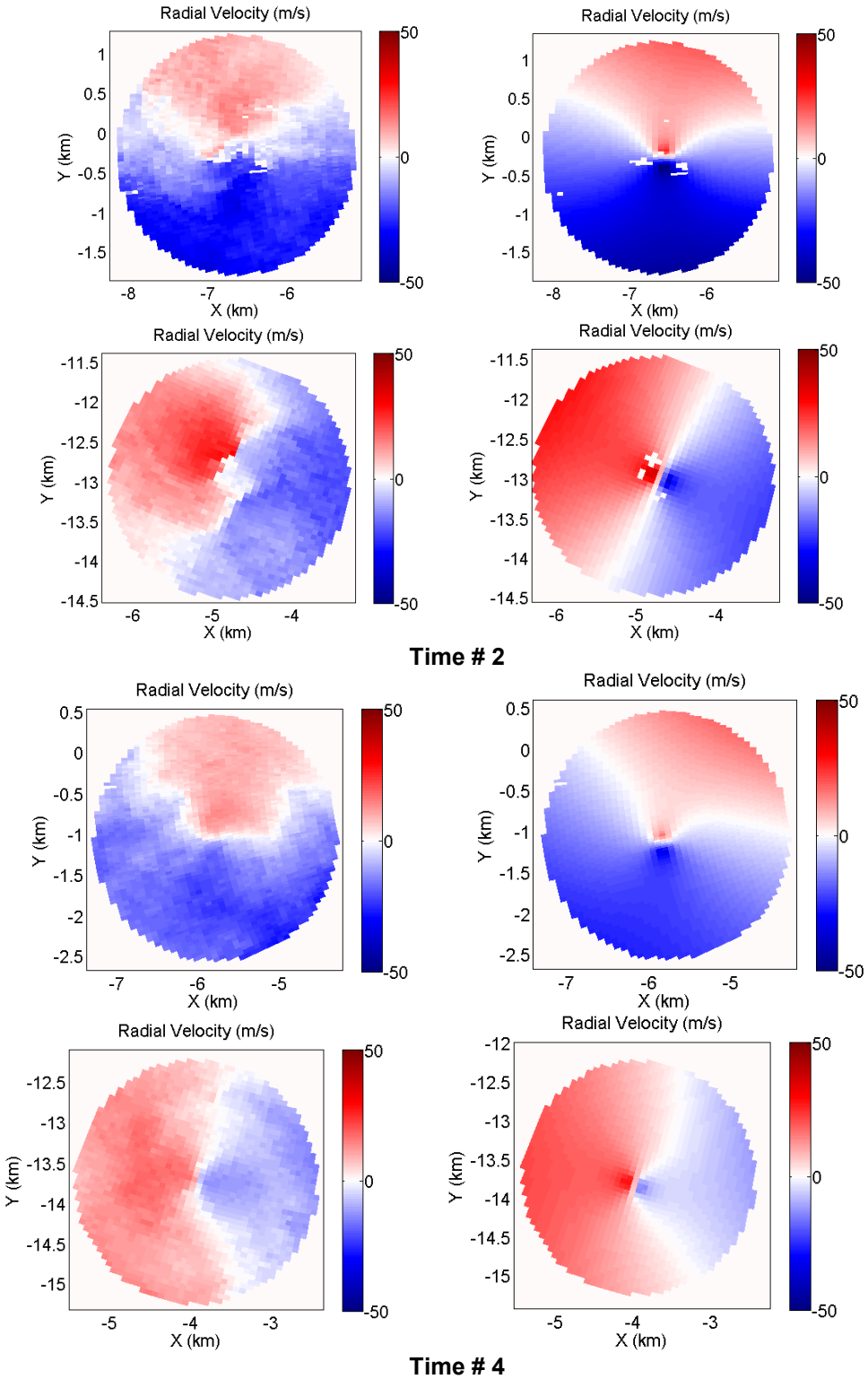

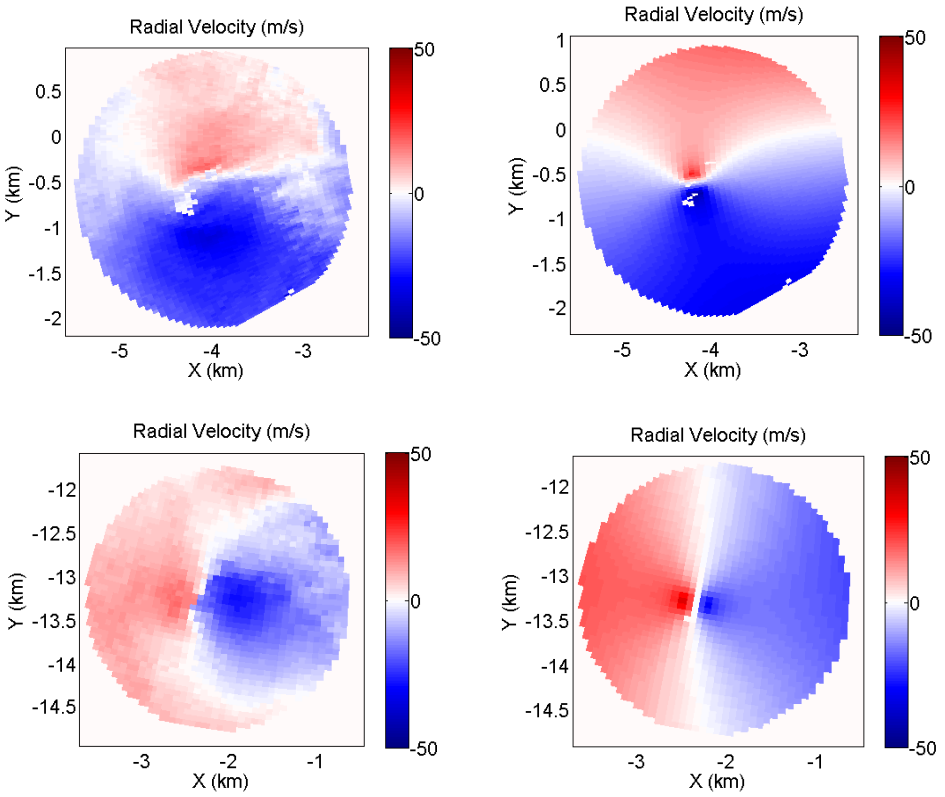
Radial Velocity (m/s)
Y (km)
X (km)
50
0
-50

Time # 6

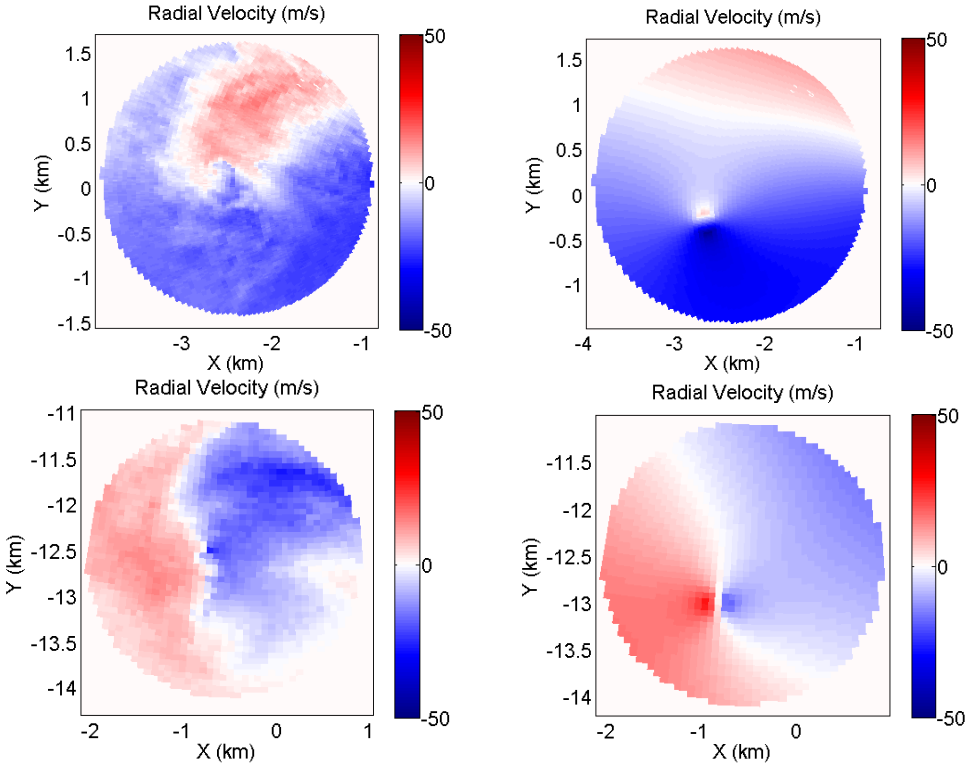
Radial Velocity (m/s)
Y (km)
X (km)
50
0
-50

Time # 8

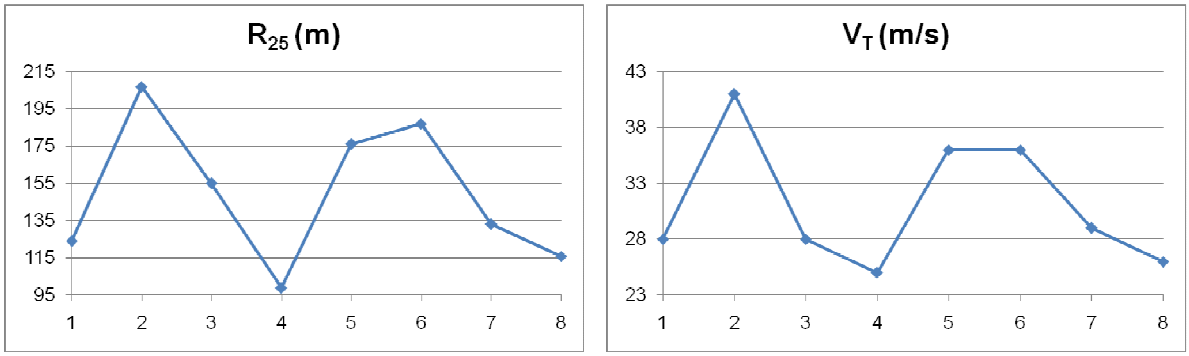

Fig. 6. Retrieved R_{25} and V_T at eight consecutive times.

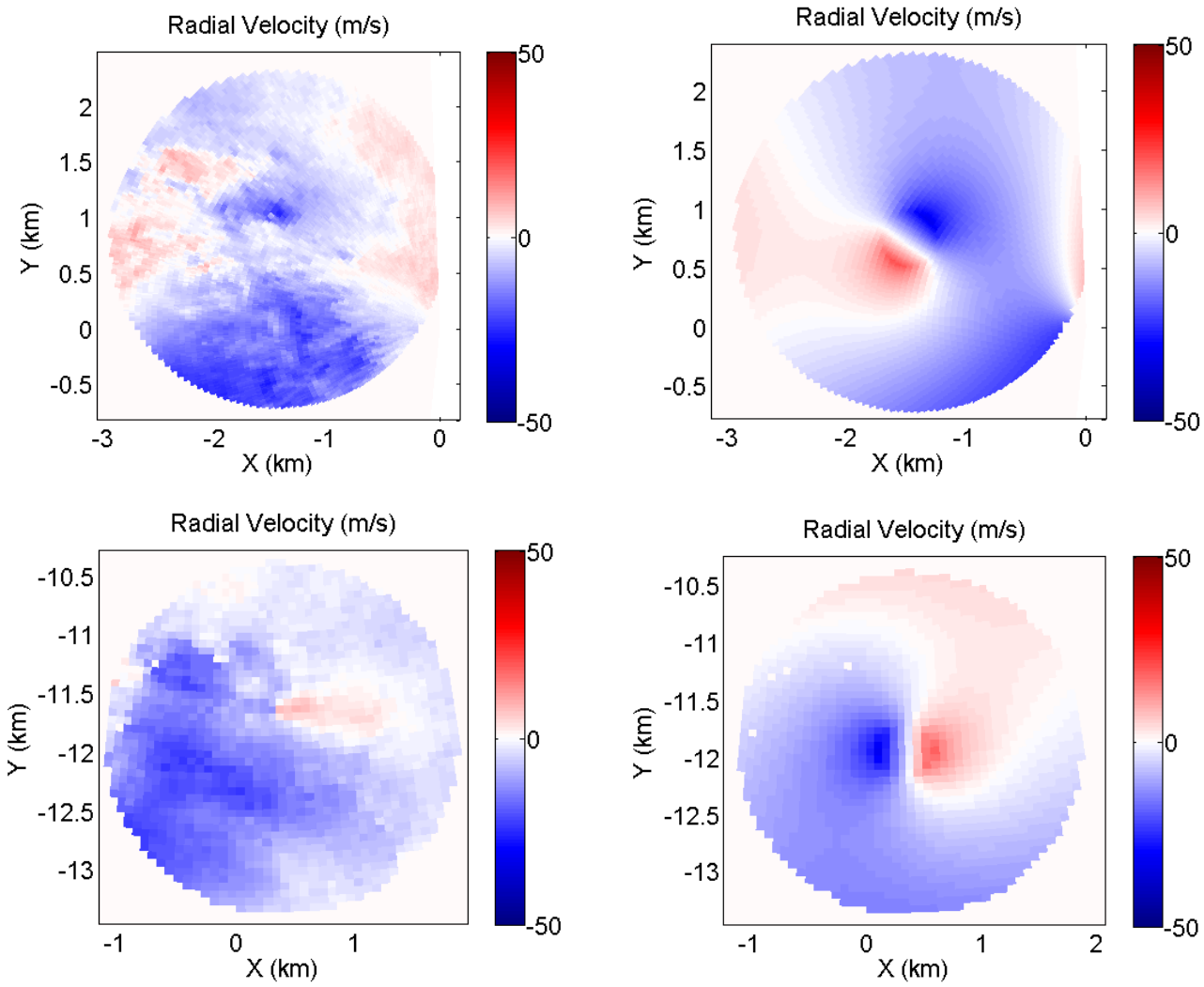

Fig. 7. Same as Fig. 5 except for a region located well away from the suspected tornado at time # 7.